Journal of Materials Chemistry A

ROYAL SOCIETY OF CHEMISTRY

PAPER

View Article Online
View Journal | View Issue

Cite this: *J. Mater. Chem. A*, 2021, **9**, 7048

Lanthanum nanocluster/ZIF-8 for boosting catalytic CO_2/glycerol conversion using $MgCO_3$ as a dehydrating agent†

Chechia Hu, *[ab] Chien-Wei Chang,[b] Masaaki Yoshida[cd] and Ke-Hsuan Wang[e]

Received 23rd December 2020
Accepted 8th February 2021

DOI: 10.1039/d0ta12413c

rsc.li/materials-a

A lanthanum-modified zeolitic imidazolate framework (La/ZIF-8) was developed to produce glycerol carbonate using CO_2 and glycerol as raw materials. La/ZIF-8 provides a high catalytic glycerol conversion efficiency owing to its surface-attached nanoclusters of La_2O_3, which can be viewed as La^{3+}–O^{2-} pairs that strengthen the Lewis basicity and acidity, and the large specific surface area of ZIF-8. The catalytic glycerol conversion and the yield of glycerol carbonate were 46.5% and 35.3%, respectively, using CH_3CN as a dehydrating agent. With increase in the amount of CH_3CN, the water molecules could react with CH_3CN to reduce the selectivity. When an inorganic dehydrating agent, $MgCO_3$, was used to physically adsorb and remove water molecules in the reaction, the selectivity of the reaction could be increased to over 95%, which is the highest ever reported. Reaction kinetics analysis also revealed that the activation energy of using $MgCO_3$ (5.4 kJ mol^{-1}) as a dehydrating agent is lower than that using CH_3CN (7.8 kJ mol^{-1}). Moreover, the La/ZIF-8 could be recycled and reused at least three times with high catalytic performance. This study provides an effective material with dual Lewis basicity and acidity for CO_2/glycerol conversion and significantly improves the catalytic performance using an inorganic dehydrating agent.

1. Introduction

Carbon dioxide (CO_2) is a major greenhouse gas that causes a rise in global temperatures and strongly affects human activities and our environment. Researchers worldwide have explored several approaches to reduce CO_2 emission or to convert CO_2 into valuable chemicals including cyclic carbonates, polycarbonates, formic acid, methane, and methanol through heterogeneous catalysis.[1–4] Among these reactions, catalytic CO_2 conversion with the addition of glycerol (GL) is desirable and attracts considerable attention because GL is also an abundant by-product of the transesterification of triglycerides with methanol to produce biodiesel. Moreover, GL has been oversupplied in the world market, resulting in a sharp drop in its price, and hence it should be converted to high-value chemicals (Fig. 1(a)). In this regard, a value-added strategy to convert CO_2 with GL to produce glycerol carbonate (GLC) using heterogeneous catalysts as a valuable product is a promising alternative.[5–7] The desirable product of catalytic CO_2/GL conversion is GLC, which requires removing water continuously in the reaction to increase the conversion and yield (Fig. 1(b)). In addition, the conversion and yield of the catalytic CO_2/GL reaction are still low because of its thermodynamic limitation ($\Delta G = 23.92$ kJ mol^{-1}). Generally, acetonitrile, 4-cyanopyridine, and its derivatives could serve as dehydrating agents in increasing both the conversion and yield of the catalytic CO_2/GL reaction.[8–10] However, the addition of these dehydrating agents often leads to the formation of several by-products, including acetic acid, diacetin, or monoacetin, as shown in Fig. 1(b). To the best of our knowledge, very few studies have been reported that improve the conversion, yield, and selectivity of this reaction through the addition of inorganic dehydrating agents, such as $MgCO_3$ and $CaCO_3$. Park *et al.* examined the influence of various inorganic dehydrating agents (ZnO, MgO, and CaO) on the synthesis of dimethyl carbonate *via* oxidative carbonylation of methanol and showed that the methanol conversion and the selectivity of dimethyl carbonate can be improved when using these inorganic dehydrating agents.[11] Other inorganic dehydrating agents (KOH, $ZnCl_2$) have also been employed in the chemical activation to prepare activated carbon.[12]

[a]*Department of Chemical Engineering, National Taiwan University of Science and Technology, Daan Dist., Taipei City, 106, Taiwan. E-mail: chechia@mail.ntust.edu.tw; Fax: +886-2-27376644; Tel: +886-2-27376638*

[b]*Department of Chemical Engineering, R&D Center for Membrane Technology, Luh Hwa Research Center for Circular Economy, Chung Yuan Christian University, Chungli Dist., Taoyuan City, Taiwan 320*

[c]*Applied Chemistry, Graduate School of Sciences and Technology for Innovation, Yamaguchi University, Ube, Yamaguchi, 755-8611, Japan*

[d]*Blue Energy Center for SGE Technology (BEST), Yamaguchi University, Ube, Yamaguchi 755-8611, Japan*

[e]*Department of Industrial Chemistry, Tokyo University of Science, Shinjuku-ku, Tokyo, 162-8601, Japan*

† Electronic supplementary information (ESI) available. See DOI: 10.1039/d0ta12413c

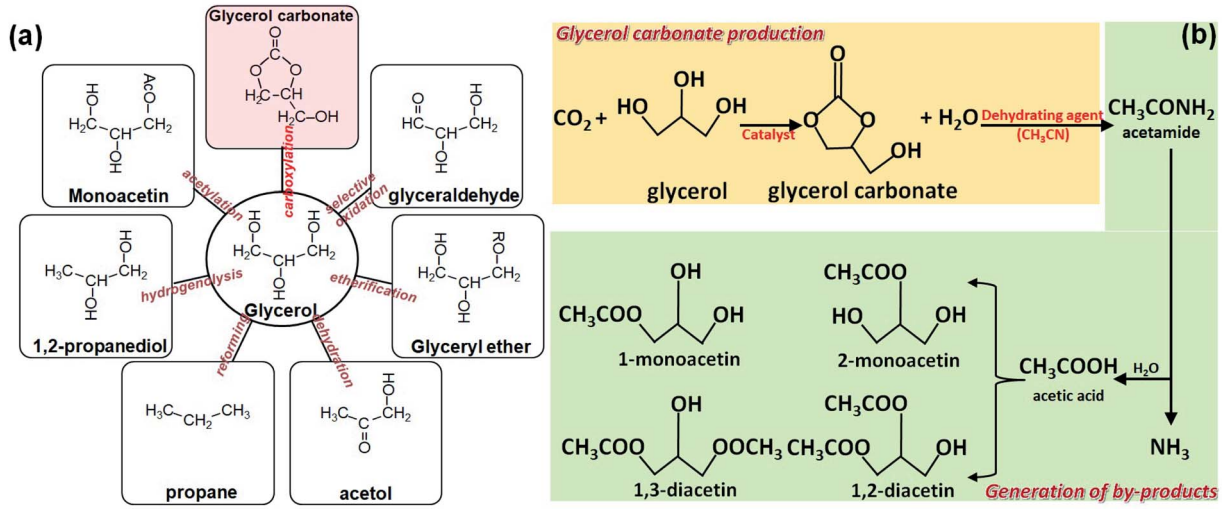

Fig. 1 (a) Glycerol conversion reactions to yield high-value chemicals, including carboxylation of glycerol to produce glycerol carbonate. (b) Overall catalytic CO_2/glycerol conversion in the presence of a dehydrating agent (CH_3CN) and catalyst to yield glycerol carbonate as the main product and the generation of by-products including 1-monoacetin, 2-monoacetin, 1,3-diacetin, and 1,2-diacetin.

It is vital to develop a novel material for the utilization, reduction, and catalytic conversion of a greenhouse gas (CO_2) through heterogeneous catalysis. Unlike commonly used homogeneous catalysts such as NaOH, CH_3OK, and K_2CO_3, which are dissolved in the GL solution and are difficult to be recycled, heterogeneous catalysts could be easily separated from the products and reused, reducing the operation cost. In recent years, many heterogeneous catalysts including metal oxides (ZnO, ZrO_2, and CeO_2)[13–15] and metal complexes[16] have shown potential in the CO_2/GL reaction as shown in Table 1.[9,17–27] However, the selectivity and yield of GLC using heterogeneous catalysts are still poor due to the absence of either Lewis basic or acidic sites, relatively small surface area, and weak CO_2 affinity. For better utilization of heterogeneous catalysis for CO_2/GL conversion, materials with large surface area, ease of modification, and strong CO_2 affinity are required. Zeolite and metal–organic frameworks (MOFs) with mesoporous nature and abundant surface functional groups are considered as potential candidates for this reaction.[28,29] Moreover, zeolitic imidazolate framework-8 (ZIF-8), which has tetrahedrally coordinated Zn^{2+} with four imidazolate units in a sodalite topology, is extensively used in catalysis, photocatalysis,[30–33] CO_2 adsorption,[34–36] gas separation,[37] sensors,[38] and supercapacitors.[39] Owing to its high CO_2 capture capability, ZIF-8 could be a potential catalyst for CO_2 conversion reaction if it is modified with an appropriate reagent to a certain extent. Many studies have reported that the introduction of lanthanum (La) ion could strengthen the surface acidity and basicity of the catalyst to increase its catalytic activity.[40] Choudhary *et al.* reported that the surface acidity and basicity of many oxide catalysts, including La_2O_3, CeO_2, Yb_2O_3, and Eu_2O_3, by NH_3-TPD (temperature-programmed desorption) and thermal desorption of CO_2, respectively, can be correlated with the surface reactivity of the catalyst for the oxidative coupling of methane reaction.[41] In addition, Lacombe *et al.* has shown that the La^{3+}–O^{2-} pair site could be critical to activate the heterolytic splitting of the CH_3–H bond.[42] Dibenedetto has studied the carboxylation of GL using *n*-$Bu_2Sn(OCH_3)_2$ as a catalyst in toluene as the solvent, which suggests that Sn could play an important role in activating CO_2 to generate GLC.[43] McGregor *et al.* suggested that an alternative pathway to increase the selectivity and yield of GL carboxylation is an acid–base reaction[27] that improves the surface basicity and acidity of the catalyst. Although ZIF-8 is widely used as a catalyst to improve the selectivity for the hydrogenation of acetylene,[44] activity of transesterification,[45] aminocarbonylation,[46] and CO oxidation,[47] no studies have reported the modification of ZIF-8 using lanthanum as a catalyst for CO_2/GL conversion and thereby determining the effect of inorganic dehydrating agents in this reaction.

In this study, La-modified ZIF-8 was prepared for the catalytic CO_2/GL reactions. La-modified ZIF-8 exhibited high catalytic activity compared to La-modified ZnO; this can be attributed to its large specific surface area and strengthened Lewis basicity and acidity. The highest conversion and yield achieved for La-modified ZIF-8 was 46.5% and 35.3%, respectively, when CH_3CN was used as the dehydrating agent. Moreover, the selectivity reached over 92% when $MgCO_3$ substituted CH_3CN was used as the dehydrating agent to remove the water molecule. This study not only reports the correlation between the improvement of the catalytic performance of La/ZIF-8 with the effect of a dehydrating agent for the first time but also provides new insights for use of metal modified MOFs to develop efficient utilization for CO_2 economy.

2. Experimental

2.1 Preparation of the catalysts

La-modified ZIF-8 was prepared by the addition of $Zn(NO_3)_2$ (>99%, Showa, Japan) and $La(NO_3)_3$, (>98%, Acros Organics, USA) in different weight ratios (0, 3, 5, 7, and 10 wt% (La/Zn)),

Table 1 Conversion, yield, and the reaction conditions of catalytic CO_2/glycerol conversion using different heterogeneous catalysts as reported in the literature

Catalyst	Conversion (%)	Yield (%)	Reaction conditions	TOF[a] (h^{-1})	Year	Ref.
CeO_2	—	78.9%	Dehydrating agent: 2-cyanopyridine, 10 mL DMF as the solvent, 40 bar of CO_2, 150 °C for 5 h	—	2016	9
K_2CO_3	57	19	Dehydrating agent: benzonitrile, propylene glycol/dehydrating agent: 100 mmol/100 mmol, 80 bar of CO_2, 175 °C for 18 h	2.48 (K_2CO_3) 16.3 (Cs_2CO_3)	2012	17
Cs_2CO_3	44	17				
Na_2CO_3	22	8				
Li_2CO_3	6	4				
$MgCO_3$	1	—				
$CaCO_3$	2	—				
$La_2(CO_3)_3$	1	—				
$Al_2(CO_3)_3$	2	—				
$La_2O_2CO_3$–ZnO	30.3	14.3	Dehydrating agent: CH_3CN, glycerol/dehydrating agent: 50 mmol/5 mL, 40 bar of CO_2, 170 °C for 12 h	2.47 ($La_2O_2CO_3$–ZnO)	2013	18
CaO	5.3	—				
Cu/La_2O_3	33.4	15.2	Dehydrating agent: CH_3CN, glycerol/dehydrating agent = 50 mmol/10 mL, 70 bar of CO_2, 170 °C	16.7	2014	19
Cu/CaO	0.3	0.025	Dehydrating agent: CH_3CN, glycerol/dehydrating agent: 50 mmol/10 mmol, 70 bar of CO_2, 150 °C	76.4 (Cu/Mg–Al–Zr) 107.1 (Cu/MCM-41)	2015	20
Cu/MgO	8.6	2.25				
Cu/La_2O_3	8.9	2.61				
Cu/Al_2O_3	1.36	1.18				
Cu/ZrO_2	11.2	2.08				
Cu/Mg–Al–Zr	11.5	2.40				
Cu/CNTs	7.3	1.30				
Cu/MCM-41	18.7	1.83				
Cu/HZSM-5	0.5	0.07				
Halogen (F, Cl, Br) modified Zn–Al–La oxide	35.5	16	Dehydrating agent: CH_3CN, glycerol/dehydrating agent = 50 mmol/5 mL, 40 bar of CO_2, 170 °C for 12 h	1.67	2015	21
Zn-modified zeolite Y	—	5.8	Dehydrating agent: none, solvent: ethanol, glycerol/solvent = 274 mmol/30 mL, 100 bar of CO_2, 300 °C for 3 h	—	2015	22
Zn/Al/La/M (M = Li, Mg, Zr) hydrotalcites	35.7	15.1	Dehydrating agent: CH_3CN, glycerol/dehydrating agent = 50 mmol/5 mL, 40 bar of CO_2, 170 °C for 12 h	0.5	2015	23
ZnO	41.3	11.9	Dehydrating agent: 2-cyanopyridine, glycerol/dehydrating agent: 12.5 mmol/25 mmol, 100 bar of CO_2, 170 °C for 12 h	0.75 (CeO_2, nanopolyhedra)	2017	24
TiO_2	30.9	10.9				
ZrO_2	37.2	10.4				
Al_2O_3	34.5	10.5				
CeO_2 (nanopolyhedra)	35.5	14.2				
CeO_2 (mesoporous)	29.3	10.3				
CeO_2 (nanocube)	34.4	10.4				
CeO_2 (nanorods)	28.1	12.9				
CeO_2 (nanowires)	38.2	13.5				
ZrO_2–CeO_2	36.5	27.6	Dehydrating agent: 2-cyanopyridine, solvent: DMF, glycerol/dehydrating agent/solvent = 10 mmol/30 mmol/10 mL, 30 bar of CO_2, 150 °C for 5 h	0.27	2018	25
$ZnWO_4$/ZnO	17.7	12.2	Dehydrating agent: none, solvent: DMF, glycerol/solvent = 100 mmol/20 mL, 30 bar of CO_2, 150 °C for 6 h	—	2018	26
La_2O_3	58	9.9	Dehydrating agent: adiponitrile, glycerol/dehydrating agent = 22.5 mmol/45 mmol, 45 bar of CO_2, 160 °C for 18 h	0.57	2019	27

[a] TOF: turnover frequency, —: not indicated.

and 2-methylimidazole (2000 mg, 99%, Acros Organics, USA) to a methanol solution (12 mL, HPLC grade, Aencore, Australia) at ambient temperature under stirring for 1 h. The mole ratio of $La(NO_3)_3$ to 2-methylimidazole was 1 : 4. Then the suspension was centrifuged at 7000 rpm for 15 min, followed by washing with methanol solution (30 mL) three times. The resulting samples were heat-treated at 200 °C for 6 h in an air atmosphere at a ramp rate of 1.5 °C min^{-1}, and designated as *x*La/ZIF-8

hereafter, where x refers to 3, 5, 7, and 10 (weight ratios of La to Zn). For comparison, La-modified ZnO was prepared by adding $La(NO_3)_3$ to ZnO (99%, Showa, Japan), followed by heat treatment identical to the above process to yield xLa/ZnO samples.

2.2 Characterization

The crystalline structure of the specimens was identified using X-ray diffraction (XRD; Bruker D8 Advance, USA) at 2θ angles of 10°–70° with a scan rate of 6° min^{-1}. The surface morphologies and microstructures of the specimens were investigated using transmission electron microscopy (TEM; Hitachi H-7100, Japan) and scanning electron microscopy (SEM; Hitachi S–4800N, Japan). The elemental compositions of the samples were determined using an energy dispersive spectrometer equipped with SEM (SEM-EDS). The particle size of the specimens was measured using a dynamic light scattering analyzer (DLS, Zetasizer Nano S-90, Malvern, UK). The N_2 adsorption–desorption isotherms of the samples were examined at −196 °C using an adsorption apparatus (Micromeritics ASAP 2020, USA), and the specific surface areas were estimated using the Brunauer–Emmett–Teller (BET) equation. X-ray photoelectron spectroscopy (XPS; VG Scientific ESCALAB 250, Electron Spectroscopy for Chemical Analysis, UK) with Al Kα radiation was carried out to determine the electron binding energy of the products by C 1s (284.8 eV) calibration. The catalytic CO_2 conversion, selectivity, and yield obtained using the catalysts were measured by nuclear magnetic resonance (NMR, Bruker AVIII-400(B662), USA). Thermogravimetric analysis (TGA, TA Q50, DuPont) was used to investigate the thermal stability and pyrolysis temperature of ZIF-8 and La/ZIF-8 catalysts under a nitrogen flow with a heating rate of 10 °C min^{-1}. A temperature-programmed desorption analyzer (TPD; AutoChem 2920, Micromeritics, USA) was used to evaluate the basic or acidic sites of the obtained samples in a CO_2 or NH_3 atmosphere under ambient pressure. The temperature was increased from room temperature to 400 °C (ramp rate of 2 °C min^{-1}).

The La K-edge X-ray absorption fine structure (XAFS) spectra were obtained in transmission and fluorescence mode at BL01B1 in the SPring-8 facility, using radiation monochromatized with a $Si_{(311)}$ double-crystal monochromator. The ring energy and current were 8 GeV and 100 mA, respectively. In transmission mode, the intensities of the incident X-rays were monitored using ion chambers placed in front of the sample to obtain I_0 (17 cm in length) and after the sample to obtain I_1 (31 cm). The XAFS spectra of La_2O_3, and $La(OH)_3$ pellets diluted with BN powders were acquired as references. It should be noted that the La_2O_3 powders were heated at 1000 °C for 12 h just before the XAFS measurements because the stored La_2O_3 gradually transforms into $La(OH)_3$ upon exposure to moisture in the air. In fluorescence mode, the fluorescence X-ray was acquired using a 19-element equipped Ge detector (Ortec). The XAFS spectra for the prepared samples were acquired by fixing on a Scotch tape. The photon energies were calibrated from the peak of La_2O_3 (38 955 eV) for all the measurements, with reference to a previous study.[48]

2.3 Catalytic reactions

Catalytic conversion of CO_2 and GL was carried out using 0.1 g of the catalysts in a 100 mL stainless steel autoclave pressurized with CO_2 to 7 bar at a temperature of 150 °C in the presence of CH_3CN, $MgCO_3$, or $CaCO_3$ as the dehydrating agent. To determine the reaction kinetics and the activation energy by Arrhenius equation, $k = Ae^{-E_a/RT}$, where k, A, E_a, R, and T indicate the kinetic rate constant, collision frequency factor, activation energy, energy gas constant, and temperature, respectively. The reaction times and temperatures varied between 3, 6, 9, 12, and 15 h, and 120 °C, 150 °C, and 180 °C, respectively. The time-dependent C_A, $\ln(C_A/C_{A0})$, and $1/C_A$ for the 0^{th}-, 1^{st}-, and 2^{nd}-order reaction were employed to determine the rate constant (C_A refers to the glycerol concentration). After the reaction, the autoclave was cooled naturally to room temperature and the suspension was centrifuged, washed, and collected for NMR (Bruker Advance II spectrometer, USA) and GC-FID (GC-2014, Shimadzu, Japan; Column: SOLGEL-WAX) analyses to determine the conversion, yield, and selectivity. The temperatures of the oven and detector in the GC-FID system were controlled at 260 and 270 °C, respectively. The carrier gas was N_2 (total flow rate: 19.5 mL min^{-1}). The conversion, yield, and selectivity were calculated based on the following equations:

$$\text{Conversion (\%)} = (\text{mole of glycerol consumed})/(\text{initial mole of glycerol}) \times 100\% \quad (1)$$

$$\text{Yield (\%)} = (\text{mole of glycerol carbonate})/(\text{theoretical mole of glycerol carbonate}) \times 100\% \quad (2)$$

$$\text{Selectivity (\%)} = (\text{mole of glycerol carbonate produced})/(\text{mole of glycerol consumed}) \times 100\% \quad (3)$$

The catalyst and dehydrating agent used were separated by precipitation and centrifugation at 9000 rpm for 15 min, followed by washing with deionized water and dried at 80 °C for 24 h.

3. Results and discussion

3.1 XRD analysis: crystal structure of La/ZIF-8

In this study we prepared La-modified ZIF-8 samples by mixing $La(NO_3)_3$ and $Zn(NO_3)_2$ in different weight ratios with the addition of 2-methylimidazole, followed by stirring, centrifugation, and heat treatment. The XRD patterns of these prepared catalysts are shown in Fig. 2. The ZIF-8 and La/ZIF-8 powders exhibited a pure phase structure of the zeolitic imidazolate framework, whereas a small peak at approximately 31° was observed for La/ZIF-8 catalysts (Fig. 2(a)). This indicates the formation of La_2O_3(100) accompanied by the crystallization of ZIF-8. The crystallite size of La_2O_3(100) for these samples was calculated to be approximately 1 nm by Scherrer equation. This means that the La_2O_3 nanoclusters were highly dispersed on the surface of ZIF-8. The detailed review of the XRD patterns in Fig. 2(b) showed that the 2θ value of the characteristic peaks at (011), (002), and (112) for ZIF-8 and La/ZIF-8 catalysts did not shift towards higher or lower values after La-modification,

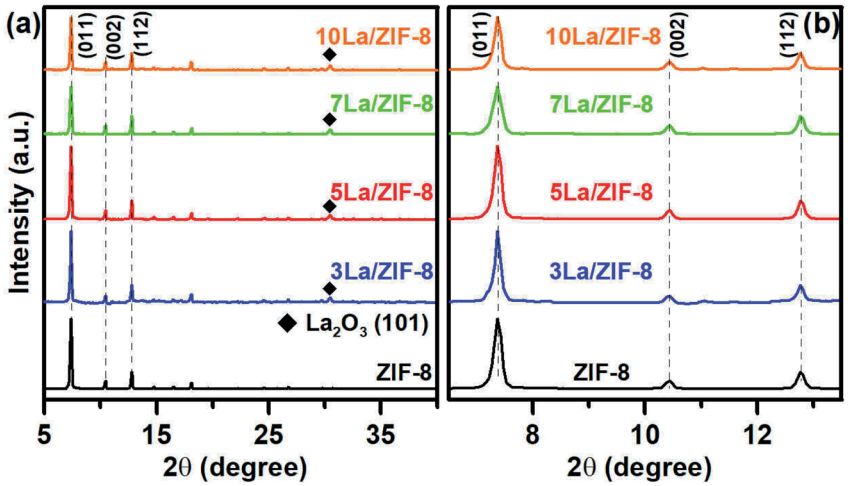

Fig. 2 (a) XRD patterns and (b) the corresponding magnified peaks of ZIF-8 and La/ZIF-8 samples.

implying that La ions did not insert into the crystal lattice nor did they substitute Zn sites in ZIF-8. We also prepared 5La/ZnO as a control group for the XRD measurement as shown in Fig. S1(a),† demonstrating its hexagonal wurtzite structure. The TGA measurements of ZIF-8, 5La/ZIF-8, and 10La/ZIF-8 are shown in Fig. S1(b).† At approximately 400–450 °C, the surface-attached methyl groups of the methylimidazolate ligands decomposed with increasing temperature; above 600 °C, the main [$MeIM_2$] framework of ZIF-8 collapsed. The residual weight of ZIF-8 is related to the zinc and lanthanum content of the catalyst, and the higher weight loss of 10La/ZIF-8 compared to those of ZIF-8 and 5La/ZIF-8 indicated its structural instability at high temperatures owing to a certain extent of La-modification.[49]

3.2 SEM, TEM images and N_2 isotherms: morphology and appearance of La/ZIF-8

SEM and TEM were used to investigate the surface morphology, appearance, and crystal structure of ZIF-8 and La/ZIF-8 samples. Fig. S2(a–c)† show the SEM images of ZIF-8, 5La/ZIF-8, and 10La/ZIF-8 powders, indicating that the particle size of ZIF-8 was primarily in the range of 100–150 nm with a hexagonal shape (Fig. S2(a)†), which is similar to that reported earlier.[50] With increased La-modification on ZIF-8, the particle size of La/ZIF-8 did not change significantly, but the particles became more circular (Fig. S2(b) and (c)†). This is primarily because La-doping could induce the inhomogeneity on the particle size and shape of ZIF-8, which is similar to Fe-doped ZIF-8 as reported in a previous study.[51] Fig. S2(d–f)† show the representative TEM images of these samples, confirming the hexagonal structure of ZIF-8 (Fig. S2(d)†) and the presence of small particles attached onto and surrounded by the periphery of the ZIF-8 particles in La/ZIF-8 powders (Fig. S2(e) and (f)†). These small particles could be attributed to the La_2O_3 clusters, which can be seen in XRD analysis at a 2θ of approximately 30.5°. HR-TEM images were taken for ZIF-8, 5La/ZIF-8, and 10La/ZIF-8 samples (Fig. 3). The nanoclusters of La_2O_3 as indicated by the arrows could be seen in Fig. 3(b and c), and the inset of Fig. 3(b), whereas no other particles were found attached on the surface of ZIF-8 in Fig. 3(a), which is consistent with the above SEM and TEM analyses. The nanoclusters of La_2O_3 have a particle size of approximately 1–3 nm, which is consistent with the above

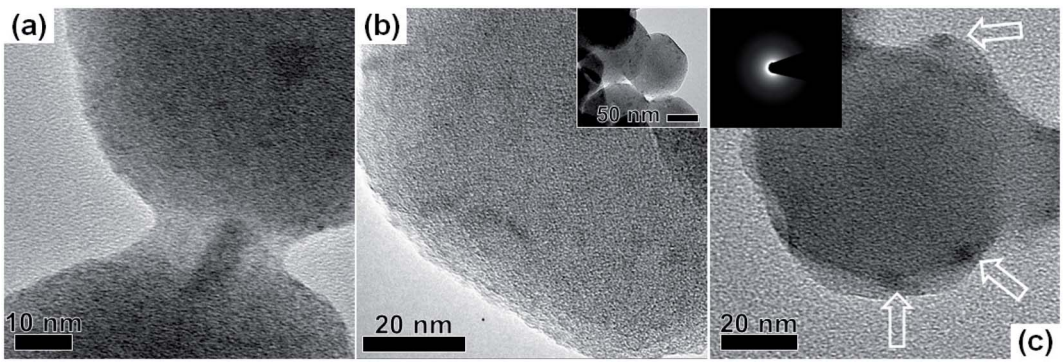

Fig. 3 HR-TEM images of (a) ZIF-8, (b) 5La/ZIF-8, and (c) 10La/ZIF-8 samples. Insets of (b) and (c) show the TEM image and the electron diffraction of the corresponding sample.

crystallite size obtained from XRD, showing the high dispersion of La_2O_3 on the surface of ZIF-8. The inset of Fig. 3(c) shows the electron diffraction of the 10La/ZIF-8 sample. The insignificant electron diffraction ring suggested the low crystallinity of 10La/ZIF-8 or the relatively small grain size of La_2O_3 attached on the ZIF-8 surface.

The N_2 adsorption–desorption isotherms of ZIF-8 and La/ZIF-8 samples are shown in Fig. S3,† illustrating their mesoporous features classified as type VI isotherms according to the IUPAC.[30,52,53] The surface areas of ZIF-8, 3La/ZIF-8, 5La/ZIF-8, 7La/ZIF-8, and 10La/ZIF-8 samples were estimated to be 1830 ± 50, 1720 ± 30, 1700 ± 20, 1680 ± 30, and 1430 ± 70 $m^2\ g^{-1}$, respectively. The lower specific surface area of La/ZIF-8 could be attributed to the surface coverage by La_2O_3 nanoclusters which hinders the N_2 diffusion and adsorption to the mesopores of ZIF-8 samples. As shown in the inset of Fig. S3,† the pore size of these samples should be smaller than 1 nm; however, broad pore width distributions for these samples were observed. This could be ascribed to the inter-particular diameter between the connected particles, which is consistent with the SEM and TEM results in Fig. S2 and S3.† Notably, the mesoporous feature of ZIF-8 and La/ZIF-8 endows more reactive sites, and thus, enhances the catalytic performance.

3.3 XPS analysis: chemical bonding of La/ZIF-8

To determine the chemical bonding and the oxidation states of La/ZIF-8 samples, XPS was performed (Fig. 4). The C 1s peak can be deconvoluted into two peaks at approximately 285.4 and 286.3 eV (Fig. 4(a)), which corresponds to C–C/C=C and C–N bond, respectively.[54] It can be noted that these peaks remained unchanged in 5La/ZIF-8 and 10La/ZIF-8 samples, indicating that the framework of ZIF-8 was well preserved after La-modification. We also observed two deconvoluted peaks at 399.1 eV and 399.8 eV in N 1s spectra (Fig. 4(b)), presenting the characteristic bonding of C=N– and C–NH– groups of ZIF-8,[55] and two prominent peaks attributed to Zn $2p_{3/2}$ and Zn $2p_{1/2}$ situated at 1022.2 eV and 1045.1 eV (Fig. 4(c)), respectively.[56] With an increase in La content, the La 3d signal increased accordingly in the range of 835–840 eV (Fig. 4(d)), implying the presence of La species on the ZIF-8 catalyst. The small peak at approximately 836.5 eV in the 5La/ZIF-8 sample can be ascribed to the La^{3+} species, whereas the two peaks at 835.5 eV and 838.2 eV are characteristic of the typical La_2O_3 as an oxide.[57] These results agreed with the XRD analysis that confirmed the presence of La_2O_3 accompanied by the crystallization of ZIF-8. Elemental analyses using SEM-EDS and XPS were performed to determine the chemical composition in La/ZIF-8 samples (Fig. S4†). It can be noted that with an increase in the La content, the atomic ratio of carbon, nitrogen, and zinc decreased slightly, whereas the lanthanum and oxygen content increased accordingly, thus confirming the formation of the La/ZIF-8 catalyst.

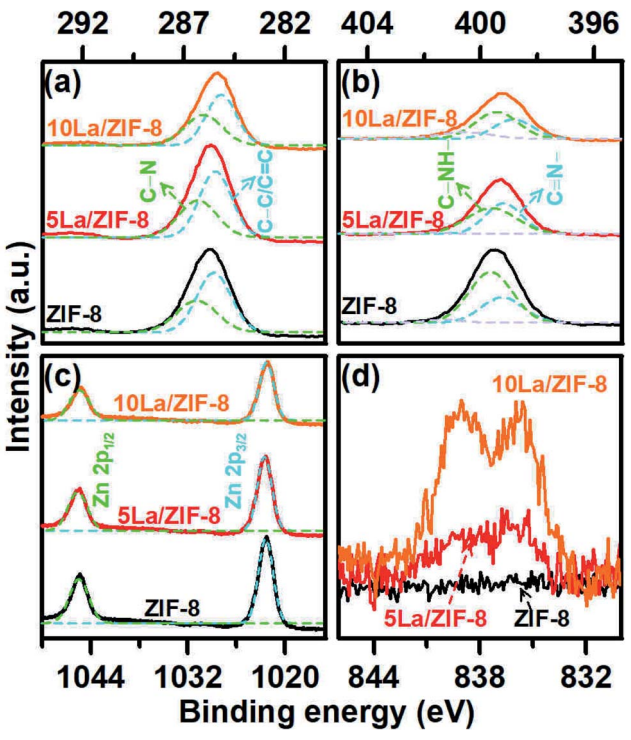

Fig. 4 High-resolution XPS spectra for (a) C 1s, (b) N 1s, (c) Zn 2p, and (d) La 3d levels of ZIF-8, 5La/ZIF-8, and 10La/ZIF-8.

3.4 XAFS analysis: nanostructure of La/ZIF-8

To investigate the electronic state and local structure of La species in the sample, XAFS spectra were taken for the La-modified ZIF-8, together with those of La_2O_3 and $La(OH)_3$ as references (Fig. 5). The X-ray absorption near-edge structure (XANES) spectra revealed that the La species in the La-modified ZIF-8 were similar to those of lanthanum(III) compounds, as shown in Fig. 5(a) and its inset. Additionally, the Fourier transform magnitude of k^3-weighted extended X-ray absorption fine structure (EXAFS) spectra indicated that the first (La–O) peaks for the samples were observed at the same peak position as that for the $La(OH)_3$ (Fig. 5(b)), suggesting that the La species in the La-modified ZIF-8 is similar to that present in $La(OH)_3$. However, the second (La–La) peak was not observed for the La-modified ZIF-8, demonstrating that the La species is composed of $La(OH)_3$ nanoclusters within a few nm in size. It should be

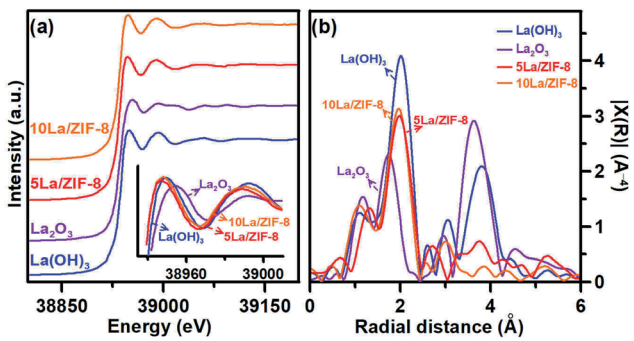

Fig. 5 (a) La K-edge XANES, (b) Fourier transform magnitude of k^3-weighted EXAFS spectra for the 5La/ZIF-8, 10La/ZIF-8, and the references of $La(OH)_3$, and La_2O_3.

noted that the La species in freshly prepared La/ZIF-8 was detected as La_2O_3 by XRD and XPS, although the La species was observed as $La(OH)_3$ by XAFS. The difference is mainly derived from the gradual change of La_2O_3 to $La(OH)_3$ on exposure to the moisture in air.[58] This was confirmed by XAFS as the stored La_2O_3 powder transformed into $La(OH)_3$ by moisture and the $La(OH)_3$ returned to the original La_2O_3 by heating at 1000 °C. Combining the structural analyses by EXAFS, XRD, and XPS, we believe that the La species in freshly prepared La/ZIF-8 exists as La_2O_3 nanoclusters within a few nm in size somewhere in or above the ZIF frame, which strengthens the Lewis acidity and basicity of the catalyst at the same time, and hence improves the activity of catalytic CO_2/GC conversion.

3.5 TPD analysis: acidity and basicity of La/ZIF-8

The CO_2- and NH_3-TPD was used to measure the surface basicities and acidities of the catalysts (Fig. 6). Typically, CO_2 chemisorption involves not only the O^{2-} site but also the La^{3+} site, which is associated with the Lewis basicity and acidity, respectively. The CO_2 desorption peaks were detected in the temperature range of 230–400 °C, indicating that the basic sites result from the CO_2-adsorption energies on ZIF-8 and La/ZIF-8 samples. The temperature above 400 °C could result in the partial decomposition of ZIF-8 and La/ZIF-8, as evidenced in TGA (Fig. S1(b)†). It can be seen that the contents of basic sites (230–400 °C) in 5La/ZIF-8 were larger than those of ZIF-8 (Fig. 6(a)). On the other hand, the acidic sites on the surface of 5La/ZIF-8 and ZIF-8 samples were estimated using NH_3-TPD (Fig. 6(b)). Notably, the acidic sites on the surface of 5La/ZIF-8 were greatly improved after La-modification, which can be ascribed to the La^{3+}–O^{2-} pairs in the La_2O_3 nanoclusters on the surface of 5La/ZIF-8. The calculated quantity of desorbed CO_2 (basic sites) and NH_3 amounts (acidic sites) of these samples are shown in Table 2. 5La/ZIF-8 exhibited stronger acidic or basic sites compared to ZIF-8 and 5La/ZnO, which act as a control group, implying that La-modified ZIF-8 has enhanced acidity and basicity, and this would be helpful to trigger the CO_2 activation for CO_2/GL conversion. More La_2O_3 on the surface of ZIF-8 (10La/ZIF-8) could reduce the exposure of La^{3+}–O^{2-} pairs, thereby reducing the acidity and basicity. However, TPD is not so reliable for measuring site densities and strengths of solid catalysts,[59] an advanced NMR method with a probe should be employed for more detailed qualitative and quantitative features[60] of the La/ZIF-8 samples in the future.

3.6 Catalytic reactions: effect of experimental conditions

In the catalytic measurement of ZIF-8 and La/ZIF-8 samples, GL was catalytically converted into GLC by reaction with 7 bar of CO_2 at 150 °C for 6 h in the presence of CH_3CN as the dehydrating agent (Fig. 7(a)). La/ZnO catalysts were also used as reference samples under the same conditions (Fig. 7(b)). The conversion of GL and selectivity of GC achieved the values of approximately 24% and 56%, respectively. Notably, the La-modified conventional ZnO catalysts had a GL conversion and GC selectivity lower than 15% and 40%, respectively (Fig. 7(b)). In comparison with the conventional catalyst La_2O_3, which had a conversion and yield of approximately 5% and 3% (Fig.-S5(a)†), respectively, 5La/ZIF-8 stands out as being particularly active toward CO_2/GL conversion amongst all the samples. This is mainly because 5La/ZIF-8 has more and stronger acidic and basic sites, resulting from the La^{3+}–O^{2-} pairs in the La_2O_3 nanoclusters, compared to that of ZIF-8 or La/ZnO (see TPD analysis in Fig. 6); and the decreased activity of 10La/ZIF-8 could be attributed to the decrease of surface area owing to coverage of La_2O_3 particles on the ZIF-8 surface, resulting in less surface metal–oxygen pairs. To examine the effects of the reaction conditions on the GL carboxylation using 5La/ZIF-8, Fig. S5 and S6† show the measured conversion and yield as a function of reaction temperature, time, and the amounts of catalyst and dehydrating agent (CH_3CN). It can be noted that the conversion and yield increased with an increase in the reaction temperature and reaction time. Most importantly, the conversion and yield could achieve the values of 45% and 35%, respectively, at a reaction temperature of 150 °C for 15 h, which are much

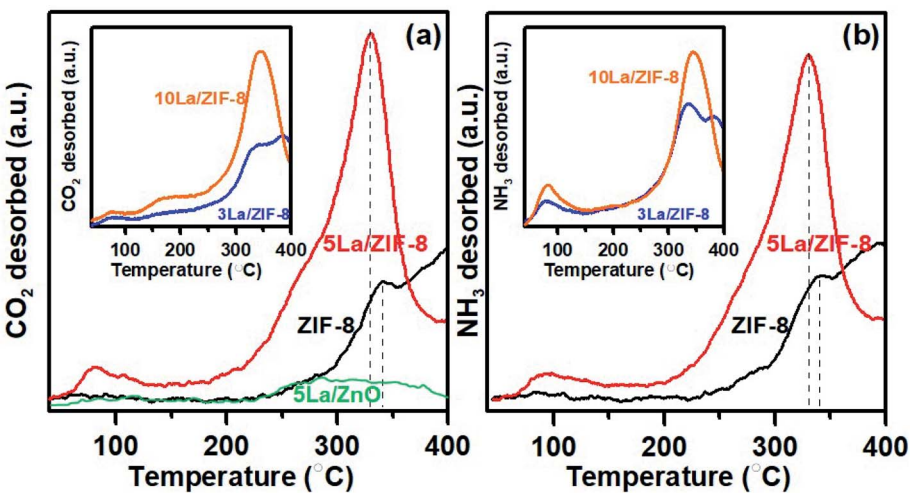

Fig. 6 (a) CO_2 and (b) NH_3 TPD plots of ZIF-8 and La/ZIF-8 samples at temperatures of 40–400 °C.

Table 2 Calculated quantity of desorbed CO_2 (basic sites) and NH_3 amounts (acidic sites) of ZIF-8 and La/ZIF-8 samples

	Desorbed CO_2 amounts (mmol g^{-1})	Desorbed NH_3 amounts (mmol g^{-1})
ZIF-8	0.121	0.158
3La/ZIF-8	0.138	0.573
5La/ZIF-8	0.305	0.582
10La/ZIF-8	0.265	0.547

higher than the reported values.[17–27] In addition, with the increase in the amount of catalyst, the conversion and yield reached a plateau, implying that the reactivity of this reaction could not be increased further by the addition of the catalyst (Fig. S6(a)†). Moreover, the yield of GL did not increase with the increase in conversion by the addition of more CH_3CN (Fig. S6(b)†). This is because more dehydrating agent may lead to undesirable side reactions and more by-products (see Fig. 1(b)). Therefore, it is necessary to determine the dehydrating efficiency and improve the catalytic performance using different reagents.

3.7 Catalytic reaction: effect of dehydrating agents

Many solvents, including acetonitrile, benzonitrile, 2-cyanopyridine, H_2SO_4, and adiponitrile, have been widely used as dehydrating agents to remove water to produce GC in the CO_2/GL conversion.[17,24,27] However, undesirable side reactions generally occurred under this circumstance. In this study, inorganic dehydrating agents, including $MgCO_3$ and $CaCO_3$, were used to remove the water by adsorption, and simultaneously restrict the side reactions in CO_2/GL conversion. Notably, the conversion, yield, and selectivity reached over 36%, 34%, and 95%, respectively, using $MgCO_3$ as the dehydrating agent in the presence of 5La/ZIF-8 under 7 bar of CO_2 at 150 °C for 15 h (Fig. 8). In addition, the selectivity was over 89% with $CaCO_3$ as the dehydrating agent, indicating that it was effective in restricting the side reactions and subsequent generation of by-products. These results correspond to the highest selectivity of CO_2/GC conversion as reported in Table 1.[17–27] However, the mechanism by which the dehydrating agent $MgCO_3$ exhibits better activity than $CaCO_3$ remains unclear. With H_2SO_4, which has dehydrating and oxidizing ability, as a dehydrating agent in this work, GC conversion was high (over 35%), but the yield of GL and the selectivity were relatively low, indicating that the major products resulted from the side-reactions. Also, ZIF-8 is unstable in an acidic environment.[61,62] Combining these results, H_2SO_4 cannot be used in this reaction.

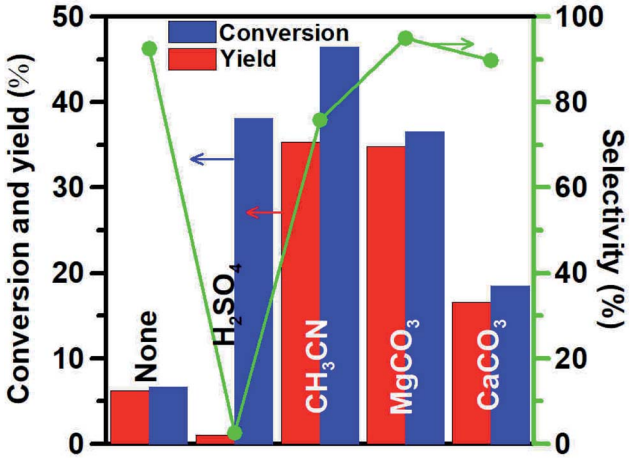

Fig. 8 Catalytic CO_2/GL conversion using different dehydrating agents including H_2SO_4 (5 mL), CH_3CN (5 mL), $MgCO_3$ (0.05 g), and $CaCO_3$ (0.05 g) in the presence of 0.1 g of 5La/ZIF-8, 15 mL of glycerol under 7 bar of CO_2 at 150 °C for 15 h.

3.8 Catalytic reactions: stability of the catalysts

The stability of the catalyst and the reusability of the inorganic dehydrating agents are important factors. We carried out the CO_2/GL conversion in the presence of 5La/ZIF-8 by adding CH_3CN, $MgCO_3$, or $CaCO_3$ as the dehydrating agent and determined its turnover frequency number (TOF), which can be expressed by the following formula:

$$\text{TOF } (h^{-1}) = (GL_0 - GL_t)/(M \times D \times T) \quad (4)$$

where GL_0, GL_t, M, D, and T refer to the moles of GL at the start and the end of the reaction time, amount of the catalyst, content of La ions obtained by XPS, and total reaction time, respectively. The TOF value of 5La/ZIF-8 in using $MgCO_3$ as the dehydrating agent is approximately 217 h^{-1}, which is higher than those in

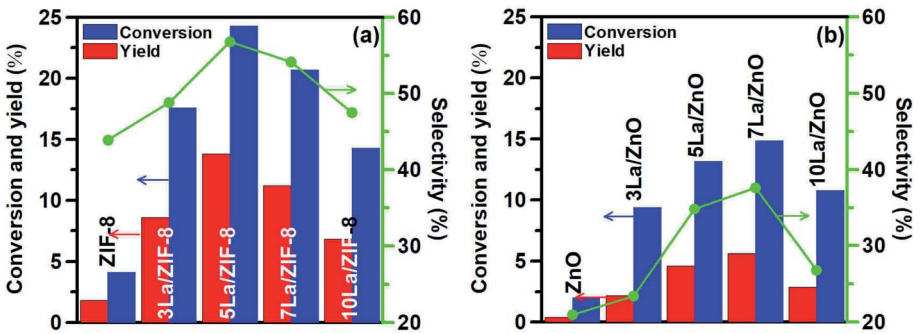

Fig. 7 Catalytic CO_2/GL conversion using (a) La/ZIF-8 and (b) La/ZnO samples as catalysts (0.1 g) at 150 °C for 6 h under 7 bar of CO_2 with 15 mL of glycerol in the presence of 5 mL of CH_3CN as the dehydrating agent.

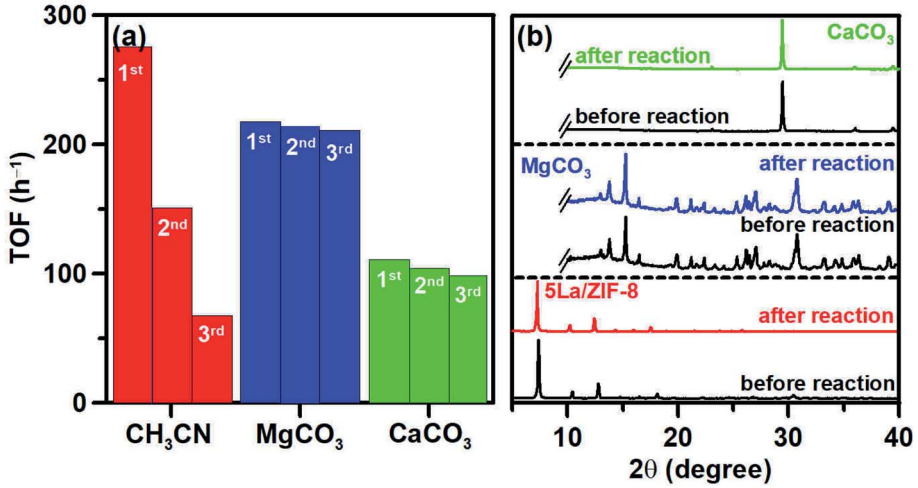

Fig. 9 (a) Repeated catalytic CO_2/GL conversion using different dehydrating agents including CH_3CN, $MgCO_3$, and $CaCO_3$ in the presence of 0.1 g of 5La/ZIF-8 as the catalyst, 15 mL of glycerol, under 7 bar of CO_2 at 150 °C for 15 h. In the reaction using $MgCO_3$ and $CaCO_3$, these dehydrating agents were recycled and reused along with the catalyst. (b) XRD patterns of 5La/ZIF-8, $MgCO_3$, and $CaCO_3$ before and after the catalytic CO_2/GL conversion.

previous results shown in Table 1. Fig. 9(a) shows the cycle test expressed in TOF using 5La/ZIF-8 with different dehydrating agents, indicating that the TOFs using $MgCO_3$ and $CaCO_3$ as dehydrating agents were maintained over 90% after three cycles, whereas the TOF decreased to approximately 40% in the case of CH_3CN. The conversion, yield, and selectivity of the cycle tests are mentioned in Table 3. This indicates that the dehydrating agents, $MgCO_3$ and $CaCO_3$, can be reused by drying to desorb the water molecules. The decreased activity could partially be attributed to the catalyst loss because La/ZIF-8 was difficult to recycle. In addition, the XRD patterns of 5La/ZIF-8, $MgCO_3$, and $CaCO_3$ remained unchanged after the CO_2/GL conversion (Fig. 9(b)). However, the particle size of 5La/ZIF-8 became smaller after the reaction, as observed by TEM imaging (Fig. S7†). Compared to the previous studies as shown in Table 1, the conversion, yield, and selectivity using 5La/ZIF-8 in the presence of $MgCO_3$ as the dehydrating agent are much higher, and hold the record for selectivity to the best of our knowledge.

Table 3 Conversion and yield of catalytic CO_2/GL conversion using 5La/ZIF-8 catalyst in the presence of different dehydrating agents[a]

Dehydrating agent		Conversion (%)	Yield (%)
CH_3CN	1st	46.5	35.3
	2nd	25.5	11.6
	3rd	11.3	5.5
$MgCO_3$	1st	36.6	34.8
	2nd	36.1	34.9
	3rd	35.6	34.1
$CaCO_3$	1st	18.5	16.6
	2nd	17.4	15.4
	3rd	16.6	14.5

[a] Reaction conditions: 15 mL of glycerol, or 0.05 g of $MgCO_3$ or $CaCO_3$ as the dehydrating agent, 0.1 g of catalyst, 150 °C, 7 bar of CO_2, 15 h.

3.9 Reaction mechanism

It is important to determine the reaction kinetics for the CO_2/GL conversion using La/ZIF-8. In this study, the linear regression for the pseudo-reaction time-dependent C_A, $\ln(C_A/C_{A0})$, and $1/C_A$ (C_A refers to the glycerol concentration, and CO_2 is excess in the reaction) for 0^{th}-, 1^{st}-, and 2^{nd}-order reaction are shown in Fig. S8(a),† illustrating that the experimental data fit 2^{nd}-order reaction kinetics with a high coefficient of determination of 0.9921. This means that the reaction could strongly be related to the concentration of the reactants. In addition, the activation energy for using CH_3CN and $MgCO_3$ as dehydrating agents, under different reaction temperatures was estimated by Arrhenius equation (Fig. S8(b)†). It is observed that the pseudo-activation energy is 7.83 kJ mol^{-1} in the case of CH_3CN, which is higher than the value obtained with $MgCO_3$ (5.42 kJ mol^{-1}). The higher activation energy suggests that the reaction is temperature sensitive and requires more external energy to activate the reaction, which is consistent with the above argument that more side reactions could occur with CH_3CN as the dehydrating agent. Most importantly, by using $MgCO_3$ as the dehydrating agent, a lower energy barrier is required for the catalytic CO_2/GL conversion. This is the first report on the catalytic activation energy of CO_2/GL conversion using the La/ZIF-8 catalyst, especially in the presence of different dehydrating agents.

The proposed reaction mechanism has been shown in Fig. 10. Glyceroxide anion is generated at the Zn sites, which serves as Lewis acidic sites, by reacting with the hydroxyl groups of GL (step 1). Then the oxygen atom on the hydroxyl group of GL attacks the Zn cations or La^{3+} sites to produce zinc glycerolate (step 2), and generates water molecules as the intermediate. Meanwhile, CO_2 molecules could be nucleophilically activated by N anions and La_2O_3 nanoclusters, which is considered as a Lewis acid–base pair for the La^{3+}–O^{2-} sites, on the catalyst surface, followed by the reaction with zinc

Fig. 10 Proposed reaction path for catalytic CO_2/GL conversion using the La/ZIF-8 sample in the presence of CH_3CN or $MgCO_3$ as the dehydrating agent.

glycerolate to produce the GLC and regenerate Zn sites at the surface (step 3). Zhao *et al.* suggested that the intra-molecular rearrangement step from glycerolate to produce glycerol carbonate could be the rate-determining step.[23] In addition, He *et al.* also demonstrated a similar reaction mechanism to indicate the importance of the acid–base property of the Ce–O pair site with low-coordinated Ce cation (as a Lewis acid site) and adjacent oxygen (as a Lewis base site) in the synthesis of propylene carbonate.[9] Moreover, the water molecules should be effectively removed by the dehydrating agent to improve the conversion, yield, and selectivity according to this reaction path. In the case of CH_3CN as the dehydrating agent, acetamide and acetic acid are generated by the reaction of CH_3CN with water molecules as by-products. With $MgCO_3$ or $CaCO_3$ as the dehydrating agent to physically adsorb water, only trace amounts of by-products are produced, resulting in a high selectivity of the GLC. As a result, the modification of La_2O_3 nanoclusters and ZIF-8 to strengthen the Lewis acidity and basicity, as well as using a dehydrating agent to physically absorb water molecules are both essential for improving the catalytic CO_2/GL conversion efficiency.

4. Conclusions

In this study, we prepared La-modified ZIF-8 as an effective catalyst for catalytic CO_2/GL conversion. After lanthanum modification, we observed La_2O_3 nanoclusters on the catalyst surface, which is confirmed by XRD, XPS, and EXAFS. These La_2O_3 nanoclusters contained a La^{3+}–O^{2-} pair site, which is considered as a Lewis acid–base site that provides an enhanced activation of the CO_2/GL reaction (evidenced by TPD). Under the optimum conditions (150 °C, 15 h, 7 bar of CO_2, 0.1 g of catalyst, 5 mL of CH_3CN as the dehydrating agent), the conversion of GL and the yield of GLC were 45% and 35%, respectively. To restrict the yield of by-products, we used $MgCO_3$ and $CaCO_3$, which could physically adsorb water molecules, as dehydrating agents. The conversion, yield, and selectivity under the optimum conditions were approximately 35%, 32.5%, and 92%, respectively, in the presence of $MgCO_3$ as the dehydrating agent by using 5La/ZIF-8 as the catalyst. The intensity of Lewis acidity and basicity could be increased by the modification of La_2O_3 nanoclusters on ZIF-8, which accepted and donated more electrons for the CO_2/GL conversion to produce GLC. The CO_2/GL conversion can be viewed as a 2nd-order reaction with activation energies of 7.83 and 5.42 kJ mol^{-1} with CH_3CN and $MgCO_3$ as dehydrating agents, respectively. In conclusion, La/ZIF-8 can be used as an effective and efficient catalyst to convert greenhouse gases (CO_2) and oversupplied GL to a high-value GLC to achieve a sustainable and green society.

Conflicts of interest

The authors declare that there is no conflict of interest.

Acknowledgements

This research was supported by the Ministry of Science and Technology, Taiwan (MOST 107-2221-E-011-156-MY3, 108-2221-E-011-165-MY3). The La K-edge X-ray absorption fine structure (XAFS) spectra were obtained at the SPring-8 (2019A1386), and Prof. Masaaki Yoshida was financially supported by Kiban C (17K05843) and the Electric Technology Research Foundation of Chugoku.

References

1 K. Li, B. Peng and T. Peng, *ACS Catal.*, 2016, **6**, 7485–7527.
2 A. Primo, J. He, B. Jurca, B. Cojocaru, C. Bucur, V. I. Parvulescu and H. Garcia, *Appl. Catal., B*, 2019, **245**, 351–359.
3 J. Xiong, P. Song, J. Di and H. Li, *Appl. Catal., B*, 2019, **256**, 117788.
4 C. Hu, H. X. Huang, Y. F. Lin, K. L. Tung, T. H. Chen and L. Lo, *Catal. Sci. Technol.*, 2019, **9**, 3800–3811.
5 S. Bagheri, N. M. Julkapli and W. A. Yehye, *Renewable Sustainable Energy Rev.*, 2015, **41**, 113–127.
6 X. Song, Y. Wu, D. Pan, J. Zhang, S. Xu, L. Gao, R. Wei and G. Xiao, *J. CO2 Util.*, 2018, **28**, 326–334.
7 J. Ma, J. Song, H. Liu, J. Liu, Z. Zhang, T. Jiang, H. Fan and B. Han, *Green Chem.*, 2012, **14**, 1743–1748.

8 J. AL-Kurdhani, H. Wang and E. Elhaj, *J. Mater. Sci. Eng.*, 2019, **8**, 2.
9 J. Liu, Y. Li, J. Zhang and D. He, *Appl. Catal., A*, 2016, **513**, 9–18.
10 M. C. J. D. Ribamar, R. C. Santos, L. P. Coutinho, O. R. Silva, H. O. Barros, V. N. Freire and A. Valentini, *Catal. Today*, 2020, **344**, 199–211.
11 D. H. Lee, J. You, J. M. Woo, J. Y. Seo, Y. C. Park, J. S. Lee, H. Kim, J. H. Moon and S. B. Park, *Chin. J. Chem. Eng.*, 2018, **26**, 1059–1063.
12 T. Ahmad, M. Danish, M. Rafatullah, A. Ghazali, O. Sulaiman, R. Kashim and M. N. M. Ibrahim, *Environ. Sci. Pollut. Res.*, 2012, **19**, 1464–1484.
13 C. Y. Park, H. Nguyen-Phu and E. W. Shin, *Mol. Catal.*, 2017, **435**, 99–109.
14 C. H. Zhou, H. Zhao, D. S. Tong, L. M. Wu and W. H. Yu, *Catal. Rev.*, 2013, **55**, 369–453.
15 M. Pagliaro, R. Ciriminna, H. Kimura, M. Rossi and C. D. Pina, *Angew. Chem., Int. Ed.*, 2007, **46**, 4434–4440.
16 P. Okoye and B. Hameed, *Renewable Sustainable Energy Rev.*, 2016, **53**, 558–574.
17 E. D. Silva, W. Dayoub, G. Mignani, Y. Raoul and M. Lemaire, *Catal. Commun.*, 2012, **29**, 58–62.
18 H. Li, D. Gao, P. Gao, F. Wang, N. Zhao, F. Xiao, W. Wei and Y. Sun, *Catal. Sci. Technol.*, 2013, **3**, 2801–2809.
19 J. Zhang and D. He, *J. Colloid Interface Sci.*, 2014, **419**, 31–38.
20 J. Zhang and D. He, *J. Chem. Technol. Biotechnol.*, 2015, **90**, 1077–1085.
21 H. Li, C. Xin, X. Jiao, N. Zhao, F. Xiao, L. Li, W. Wei and Y. Sun, *J. Mol. Catal. A: Chem.*, 2015, **402**, 71–78.
22 L. P. Ozorio, R. Pianzolli, L. D. C. Machado, J. L. Miranda, C. C. Turci, A. C. Guerra, E. F. Souza-Aguiar and C. J. A. Mota, *Appl. Catal., A*, 2015, **504**, 187–191.
23 H. Li, X. Jiao, L. Li, N. Zhao, F. Xiao, W. Wei, Y. Sun and B. Zhang, *Catal. Sci. Technol.*, 2015, **5**, 989–1005.
24 X. Su, W. Lin, H. Cheng, C. Zhang, Y. Wang, X. Yu, Z. Wu and F. Zhao, *Green Chem.*, 2017, **19**, 1775–1781.
25 J. Liu, Y. Li, H. Liu and D. He, *Biomass Bioenergy*, 2018, **118**, 74–83.
26 J. Liu and D. He, *J. CO2 Util.*, 2018, **26**, 370–379.
27 N. Razali, M. Conte and J. McGregor, *Catal. Lett.*, 2019, **149**, 1403–1414.
28 S. Hu, M. Liu, F. Ding, C. Song, G. Zhang and X. Guo, *J. CO2 Util.*, 2016, **15**, 89–95.
29 D. Wang, R. Huang, W. Liu, D. Sun and Z. Li, *ACS Catal.*, 2014, **4**, 4254–4260.
30 C. Hu, Y. C. Huang, A. L. Chang and M. Nomura, *J. Colloid Interface Sci.*, 2019, **553**, 372–381.
31 O. Karagiaridi, M. B. Lalonde, W. Bury, A. A. Sarjeant, O. K. Farha and J. T. Hupp, *J. Am. Chem. Soc.*, 2012, **134**, 18790–18796.
32 N. Wei, R. X. Zuo, Y. Y. Zhang, Z. B. Han and X. J. Gu, *Chem. Commun.*, 2017, **53**, 3224–3227.
33 N. Wei, Y. Zhang, L. Liu, Z. B. Han and D. Q. Yuan, *Appl. Catal., B*, 2017, **219**, 603–610.
34 J. Cardoso, S. Stulp, J. De Brito, J. Flor, R. Frem and M. Zanoni, *Appl. Catal., B*, 2018, **225**, 563–573.
35 L. Liu, S. M. Wang, Z. B. Han, M. Ding, D. Q. Yuan and H. L. Jiang, *Inorg. Chem.*, 2016, **55**, 3558–3565.
36 I. U. Khan, M. H. D. Othman, A. Jilani, A. F. Ismail, H. Hashim, J. Jaafar, M. A. Rahman and G. U. Rehman, *Arabian J. Chem.*, 2018, **11**, 1072–1083.
37 D. Liu, X. Ma, H. Xi and Y. Lin, *J. Membr. Sci.*, 2014, **451**, 85–93.
38 E. X. Chen, H. Yang and J. Zhang, *Inorg. Chem.*, 2014, **53**, 5411–5413.
39 X. M. Cao and Z. B. Han, *Chem. Commun.*, 2019, **55**, 1746–1749.
40 C. Chu, Y. Zhao, S. Li and Y. Sun, *Phys. Chem. Chem. Phys.*, 2016, **8**, 16509–16517.
41 V. Choudhary and V. Rane, *J. Catal.*, 1991, **130**, 411–422.
42 S. Lacombe, H. Zanthoff and C. Mirodatos, *J. Catal.*, 1995, **155**, 106–116.
43 M. Aresta, A. Dibenedetto, F. Nocito and C. Pastore, *J. Mol. Catal. A: Chem.*, 2006, **257**, 149–153.
44 J. Yang, F. Zhang, H. Lu, X. Hong, H. Jiang, Y. Wu and Y. Li, *Angew. Chem.*, 2015, **127**, 11039–11043.
45 Y. Jeon, W. S. Chi, J. Hwang, J. H. Kim and Y. G. Shul, *Appl. Catal., B*, 2019, **242**, 51–59.
46 T. T. Dang, Y. Zhu, J. S. Ngiam, S. C. Ghosh, A. Chen and A. M. Seayad, *ACS Catal.*, 2013, **3**, 1406–1410.
47 H. L. Jiang, B. Liu, T. Akita, M. Haruta, H. Sakurai and Q. Xu, *J. Am. Chem. Soc.*, 2009, **131**, 11302–11303.
48 T. Yamamoto, T. Hatsui, T. Matsuyama, T. Tanaka and T. Funabiki, *Chem. Mater.*, 2003, **15**, 4830–4840.
49 Y. Pan, Y. Liu, G. Zeng, L. Zhao and Z. Lai, *Chem. Commun.*, 2011, **47**, 2071–2073.
50 R. Jin, Z. Bian, J. Li, M. Ding and L. Gao, *Dalton Trans.*, 2013, **42**, 3936–3940.
51 X. Wang, H. Zhang, H. Lin, S. Gupta, C. Wang, Z. Tao, H. Fu, T. Wang, J. Zheng and G. Wu, *Nano Energy*, 2016, **25**, 110–119.
52 R. Guillet-Nicolas, F. Bérubé, M. Thommes, M. T. Janicke and F. Kleitz, *J. Phys. Chem. C*, 2017, **121**, 24505–24526.
53 C. V. Nguyen, S. Lee, Y. G. Chung, W. H. Chiang and K. C. W. Wu, *Appl. Catal., B*, 2019, **257**, 117888.
54 M. Zhang, Q. Shang, Y. Wan, Q. Cheng, G. Liao and Z. Pan, *Appl. Catal., B*, 2019, **241**, 149–158.
55 K. Zhu, C. Chen, H. Xu, Y. Gao, X. Tan, A. Alsaedi and T. Hayat, *ACS Sustainable Chem. Eng.*, 2017, **5**, 6795–6802.
56 Y. Yin, B. Hu, X. Li, X. Zhou, X. Hong and G. Liu, *Appl. Catal., B*, 2018, **234**, 143–152.
57 J. P. H. Li, X. Zhou, Y. Pang, L. Zhu, E. I. Vovk, L. Cong, A. P. van Bavel, S. Li and Y. Yang, *Phys. Chem. Chem. Phys.*, 2019, **21**, 22351–22358.
58 P. Fleming, R. A. Farrell, J. D. Holmes and M. A. Morris, *J. Am. Ceram. Soc.*, 2010, **93**, 1187–1194.
59 R. J. Gorte and S. P. Crossley, *J. Catal.*, 2019, **375**, 524–530.
60 X. Yi, H. H. Ko, F. Deng, S. B. Liu and A. Zheng, *Nat. Protoc.*, 2020, **15**, 3527–3555.
61 Y. Lo, C. H. Lam, C. W. Chang, A. C. Yang and D. Y. Kang, *RSC Adv.*, 2016, **6**, 89148–89156.
62 Y. L. Li, H. Y. Chi, M. Y. Kan, S. Y. Pao, Y. H. Kang, J. J. Chen and D. Y. Kang, *ChemNanoMat*, 2017, **3**, 902–908.

